Equilibrated Adsorption of CO on Silica-Supported Pt Catalysts

Sergei G. Podkolzin,[†] Jianyi Shen,[†,‡] Juan J. de Pablo,[†] and James A. Dumesic*[,†]

Department of Chemical Engineering, University of Wisconsin, Madison, Wisconsin 53705

Received: October 28, 1999; In Final Form: February 14, 2000

Microcalorimetric and infrared spectroscopic studies of CO adsorption on Pt/SiO_2 were conducted at temperatures from 298 to 673 K. The adsorption of CO on silica-supported Pt is equilibrated at 673 K, and the microcalorimetric and spectroscopic results obtained at this elevated temperature are in agreement with results reported for Pt(111) at 300 K. The heat of CO adsorption decreases with coverage from the initial value of 190−180 kJ/mol to 75 kJ/mol at the saturation CO coverage of 0.7 ML. In addition, the IR band for CO adsorbed on atop sites shifts to higher wavenumbers, and the ratio of integral absorbances of bridge-bonded and atop-bonded species changes with CO coverage. At temperatures lower than 673 K, the adsorption of CO on Pt/SiO_2 is not equilibrated, and the microcalorimetric and IR spectroscopic data are essentially independent of the apparent CO coverage. A Monte Carlo simulation model was used to consolidate data for CO adsorption on Pt/SiO_2 and Pt(111). The simulation was based on a set of parameters describing the energetics for the formation of atop- and bridge-bonded CO species on a clean surface and lateral pairwise interactions between these species on a two-dimensional hexagonal lattice representing a Pt(111) surface.

1. Introduction

The adsorption of carbon monoxide on platinum surfaces has been widely studied, as summarized in recent publications.[1−4] For example, studies of CO adsorption on single-crystal platinum surfaces typically address bonding geometries and energetics, and studies of supported platinum typically employ the adsorption of CO to probe the number and nature of surface metal sites. An important difference between these studies of single-crystal surfaces and supported catalysts is that whereas adsorbed CO can equilibrate by surface diffusion on a single-crystal Pt surface at temperatures above 100 K, the CO species adsorbed on a supported Pt particle are confined to that particle at temperatures below about 600 K, where the rate of CO desorption into the gas phase is negligible.

In the present paper, we use microcalorimetric measurements and infrared spectroscopy to study the adsorption of CO on a Pt/SiO_2 catalyst in the temperature range from room temperature to 673 K. In this work, we explore the effects of the nonequilibrated nature of CO adsorption on our Pt/SiO_2 catalyst that arise from the inability of adsorbed species to migrate from one Pt particle on the support to another. We also compare the behavior of CO adsorption on Pt single-crystal surfaces with the results from our studies of CO adsorption on Pt/SiO_2 at higher temperatures (near 673 K), where equilibration of CO with the catalyst is achieved through an adsorption and desorption equilibrium. In addition to our experimental studies, we employ a Monte Carlo simulation model to describe the equilibrated adsorption of CO on Pt. We calculate adsorption isotherms, heats of adsorption versus coverage, and surface species distributions at different temperatures using a grand canonical ensemble for a hexagonal Pt(111) lattice. The energetic parameters used in these Monte Carlo simulations for CO adsorption were based on initial estimates obtained from quantum chemical calculations using density functional theory (DFT) on a Pt_{13} cluster.

2. Background

2a. CO Adsorption on Pt(111). The adsorption of CO on platinum typically leads to linearly bonded species associated with atop sites, as well as bridge-bonded species associated with two surface Pt atoms. At temperatures below 50 K, where surface diffusion of adsorbed CO is slow, a significant amount of bridge-bonded CO can be observed at low CO coverages on single-crystal Pt surfaces (e.g., lower than 0.3 ML). The vibrational band for bridge-bonded CO disappears at these low coverages when the adsorbed species are allowed to equilibrate by annealing to 100 K.[5] Sequential dosing of CO at temperatures near 100 K confirms that atop species are formed first on Pt(111), indicating that they have a higher heat of adsorption compared to bridge-bonded CO species.[6] At temperatures from 100 to 250 K, ordered overlayer structures of adsorbed CO are observed.[2,6,7] For example, a $(\sqrt{3} \times \sqrt{3})R30°$ structure is formed at a coverage of 0.33 containing only the atop CO species, and a $c(4 \times 2)$ structure is formed at a coverage of 0.5 containing equal amounts of atop and bridge-bonded CO. There is some evidence of island formation, based on the appearance of the $c(4 \times 2)$ pattern at coverages as low as 0.35.[6] These ordered CO structures are observed only in the temperature range from about 100 to 275 K. At temperatures below 100 K, equilibration of adsorbed CO species is not achieved because of the slow rate of surface diffusion, and at temperatures higher than 260−275 K, an order−disorder transition takes place, leading to a disordered lattice fluid.[8]

At coverages exceeding half of a monolayer, compressed structures comprised of $c(4 \times 2)$ stripes separated by bands of atop species are believed to be formed.[2,6] The reported values for the CO saturation coverage are close to 0.7 ML, based on measurements of apparent sticking coefficients, IRAS, and LEED data.[2,9,10] A $c(\sqrt{3} \times \sqrt{7})$ structure at a coverage of 0.71, comprised of rows of bridge-bonded species each separated by

* Corresponding author. Fax: (608) 262-5434. E-mail: Dumesic@engr.wisc.edu.

† Department of Chemical Engineering, University of Wisconsin—Madison.

‡ Department of Chemistry, Nanjing University, Nanjing 210093, China.

10.1021/jp993833o CCC: $19.00
Published on Web 03/30/2000

two rows of atop species, is proposed to exist at full coverage, based on low-temperature LEED and IRAS studies and detailed Monte Carlo simulations.[2]

2b. Vibrational Spectra of CO Adsorbed on Pt. Integrated intensities of vibrational spectra are commonly used for semi-quantitative determination of surface species concentrations. In the case of CO adsorption on Pt, analyses of vibrational spectra are complicated because of dipole−dipole coupling between adsorbed CO species. This coupling is important between species, such as adsorbed CO, that have strong dipole moments, that are physically close to one another on the surface (i.e., at high coverage), and that have similar frequencies (within 50−100 cm^{-1}) for different adsorbed species. The dipole−dipole coupling between surface species with the same initial frequency leads to an increase in the observed absorbance compared to the sum of absorbances of the individual molecules and causes an increase in the frequency of the synchronized vibrations. For surface species having initially different frequencies, an additional effect is the absorbance intensity transfer from the species with lower initial wavenumbers to the species with the highest initial wavenumber.[11−13]

Dipole−dipole coupling between the atop and bridge-bonded CO species is small, since their characteristic frequencies are different by about 200 cm^{-1}. The characteristic frequency for atop species on Pt(111) is in the range from 2068 to 2084 cm^{-1}, and the observed frequency increases with coverage to 2086−2095 cm^{-1}. The characteristic frequency for bridge-bonded CO is about 1840 cm^{-1}. Strong dipole−dipole coupling takes place between adjacent atop CO species, leading to higher overall absorbance for these species. For example, while the ratio of the extinction coefficients for atop and bridge-bonded CO groups is close to unity for Pt carbonyl cluster compounds,[14] the strong dipole coupling for atop species on Pt surfaces leads to an apparent increase in the extinction coefficient for these atop species. Accordingly, the extinction coefficient for the atop species is approximately 1.5−2.7 times higher than for bridge-bonded CO species on Pt(111) at a total coverage of 0.5 ML.[6−8] Furthermore, dipole coupling between the atop species results in the intensity transfer from bands associated with adsorption on defect sites that have lower wavenumbers to the main band with the higher wavenumber associated with atop species adsorbed on (111) terraces. As a result, a sharp, single peak for the atop species is observed. Finally, dipole coupling between atop species causes the main absorbance peak to shift upward by about 30 cm^{-1} with increasing CO coverage, on the basis of theoretical predictions. The observed shift is actually about 20 cm^{-1}, because of the decrease in the surface binding energy with increasing coverage that causes the characteristic frequency to shift to lower wavenumbers.[12]

Dipole coupling between the bridge-bonded species is negligible, since the partial coverage of these species never exceeds 0.25 ML and they are mainly surrounded by CO species on atop sites. Consequently, the extinction coefficient of bridge-bonded CO does not increase with surface coverage. In addition, the absence of dipole coupling between bridge-bonded CO species on Pt(111) terraces and on defect sites leads to a broadening of the absorbance band for these species. For this reason, it has been suggested that the band caused by bridge-bonded CO species can be difficult to detect at low resolution, depending on the number of defects on the surface.[12]

An additional phenomenon that can alter the vibrational spectrum of adsorbed CO is the loss of symmetry of the adsorbed species at high coverages or elevated temperatures. Specifically, the atop species move in the direction of the bridge-bonded configuration, and the bridge-bonded species move in the direction of the atop configuration.[7,8] The asymmetric atop species have lower characteristic wavenumbers, and owing to dipole coupling, their vibrational intensity is transferred to the dominant peak at higher wavenumber associated with the symmetric atop species on Pt(111); therefore, the overall absorbance band remains sharp. The asymmetric bridge-bonded CO species have higher characteristic wavenumbers, and the absence of dipole coupling results in a broadening of the overall absorbance band for the bridge-bonded species.

The adsorption of CO on silica-supported Pt catalysts leads to a strong peak at 2050−2084 cm^{-1} caused by CO adsorbed on atop sites and a weak, broad band at 1850 cm^{-1} from bridge-bonded CO species. The high intensity of the atop peak is attributed to dipole coupling between absorptions from different types of atop sites, whereas the broad band from bridge-bonded CO species is interpreted as a lack of dipole coupling between peaks from CO adsorbed on different Pt crystal faces and on defect sites. The changes in the vibrational spectra caused by different preparation techniques and catalyst loadings are minor compared to the dominant features resulting from CO adsorption on Pt(111) sites.[15] Therefore, it has been suggested that regardless of the metal loading, dispersion, and preparation technique, Pt catalysts with inert supports have mainly Pt(111) morphology.[3]

3. Experimental Section

3a. Catalyst Preparation. The silica-supported Pt catalyst employed in this study was prepared by impregnation. Fumed silica powder (Cab-O-Sil, S17D, provided by Cabot Co.) was stirred in an aqueous solution of tetraamineplatinum(II) nitrate (Aldrich) to form a gel. The gel was initially dried at room temperature and then at 393 K. After drying, the sample was calcined in flowing oxygen (ca. 300 cm^3/min) at 573 K for 4 h. The platinum loading was 5.6 wt %, as determined by Galbraith Laboratories (Knoxville, TN). Transmission electron microscopy (TEM) analysis of the catalyst indicated that most of the Pt particle sizes were between 2 and 5 nm.[16] The saturation atomic hydrogen coverage for the fresh catalyst was 177 μmol/g, which corresponds to a Pt dispersion of 62%.

3b. Microcalorimetric Measurements. Microcalorimetric measurements at room temperature were made using a Setaram BT2.15D heat-flux calorimeter. The apparatus and operating procedures are described in detail elsewhere.[17] Briefly, a catalyst sample (typically 0.2 g) in a Pyrex cell was reduced in ultrahigh purity hydrogen (99.999%, Liquid Carbonic) at a flow rate of ca. 300 cm^3/min at 723 K for 8 h, and the cell was then purged with ultrahigh purity helium (99.999%, Liquid Carbonic) for 2 h at a similar flow rate. The sample was then sealed in the sidearm of the Pyrex cell, producing a capsule containing the catalyst. This capsule was broken inside a set of calorimetric cells prior to collection of CO adsorption data. Volumetric and calorimetric data were collected by dosing onto the surface 1−10 μmol quantities of CO and by monitoring the residual pressure and heat response. Carbon monoxide (99.5%, AGA, Madison, WI) was purified by passage over a bed of quartz wool at 473 K and a molecular sieves trap at 190 K.

The heat response for each dose of CO was recorded as a function of time and integrated to determine the energy released during each dose. The differential enthalpies of adsorption, ΔH_{ads}, were calculated for each dose by dividing the heat released by the amount of gas adsorbed for that dose. Differential heats of adsorption are customarily reported as positive numbers, equal to $-\Delta H_{ads}$. The time for heat equilibration and data

collection was about 45 min for each dose. The volumetric system had a dynamic vacuum of about 10^{-7} Torr, and the maximum apparent leak rate was on the order of 10^{-6} Torr per minute in a system volume of about 70 cm^3, i.e., about 10^{-6} μmol/min.

Microcalorimetric measurements in the temperature range from 473 to 673 K were made using a high-temperature heat-flux calorimeter constructed in our laboratory. The high-temperature heat transducers were manufactured by International Thermal Instruments Corp. (Del Mar, CA). The heat transducer thermopiles were made from a thermally stable gold alloy. The thermopiles are housed within two identical, cylindrically shaped ceramic cups: one cup for the sample cell and the other for the reference cell. The calorimeter heat sink is composed of three stainless steel shells, each separated by a layer of insulation, and surrounded by an outer 6-cm-thick insulation wall. The high-temperature calorimeter was calibrated at each experimental temperature using the Joule effect, i.e., by measurement of the heat signal produced from an electrical pulse of known energy.

For the high-temperature microcalorimetric experiments, a catalyst sample (typically 0.6 g) was reduced in stainless steel calorimetric cells by first heating it under hydrogen pressure of about 760 Torr to 673 K in 12 h and then introducing and evacuating doses of fresh hydrogen while the temperature was held at 673 K for 8 h. After reduction of the sample, the hydrogen was evacuated for 4 h at 673 K to the residual dynamic pressure of about 10^{-7} Torr.

Hydrogen adsorption experiments were employed to determine the number of accessible Pt atoms on the surface of the catalyst. The saturation coverage of atomic hydrogen was used to normalize the CO coverage in the microcalorimetric experiments to determine the fractional CO coverage. Hydrogen adsorption measurements were made between calorimetric runs to correct the CO adsorption data for small decreases in the Pt surface area caused by slow sintering of the Pt particles at elevated temperatures. Consequently, the CO coverage in each calorimetric run was normalized by the hydrogen saturation coverage determined for the catalyst sample after that particular run.

3c. Fourier Transform Infrared Spectroscopy. Vibrational spectra of adsorbed CO were collected using a Fourier transform infrared (FTIR) spectrometer (Mattson Galaxy 5020). A catalyst pellet (about 0.05 g) was placed into a holder inside a stainless steel cell with CaF_2 windows. The details of the cell design are given elsewhere.[16] The cell was connected to a vacuum and gas-handling system. The catalyst was reduced with ultrahigh purity hydrogen (99.999%, Liquid Carbonic) at a flow rate of ca. 100 cm^3/min. The temperature was increased from 298 to 673 K in 8 h and then kept at 673 K for 4 h. The cell was purged with ultrahigh purity helium (99.999%, Liquid Carbonic) for 2 h at a similar flow rate. The helium was evacuated at 673 K to a dynamic vacuum of 10^{-6} Torr, and the temperature was decreased to the desired experimental value. Carbon monoxide was purified in the same manner as described for the calorimetric experiments.

Infrared spectra were recorded in the absorbance mode, with 1500 scans at a resolution of 2 cm^{-1}. Each reported spectrum was obtained by first collecting a spectrum of a clean catalyst at the same experimental temperature under 760 Torr of He and then subtracting it from a spectrum of CO adsorbed on the catalyst. In addition to experiments in which IR spectra were collected after exposing the Pt/SiO_2 sample to various pressures of CO at specific temperatures, we also collected IR spectra at different temperatures for a constant CO pressure. Two such isobar series of spectra were collected at CO pressures of 0.4 and 10 Torr, i.e., by decreasing the temperature from 773 K to room temperature and collecting spectra in 50 K intervals with the cooling rate of 1 K/min between spectra. Similar to the constant temperature experiments, the spectra of adsorbed CO were obtained by subtracting the spectrum of the clean pellet in He at 760 Torr at the appropriate temperatures from the spectra of the catalyst with adsorbed CO.

3d. DFT Calculations. Quantum chemical calculations were carried out by employing density functional theory (DFT) to estimate the energetics for adsorption of CO on Pt and to probe the effects of lateral interactions between adsorbed CO species. These calculations were performed with Jaguar software (Schrodinger, Inc.) on DEC workstations. The DFT method was based on Becke's three-parameter approach (B3LYP) that combines the exact HF exchange, Slater's local functional and Becke's 1988 nonlocal gradient correction to the exchange functional, and the correlation functional of Vosko−Wilk−Nusair (VWN) and Lee−Yang−Parr (LYP).

The basis set employed in the calculations was LACVP**, which was developed at the Los Alamos National Laboratory by Hay and Wadt. This basis set uses an effective core potential on all Pt atoms. The electrons treated explicitly on Pt are the outermost core and valence electrons ($5s^25p^65d^96s^1$). The remaining core electrons are treated with effective core potentials that account for mass−velocity and relativistic effects. The electronic energy change of adsorption is defined as the difference between the energy of the cluster with the adsorbate and the energies of the cluster and the adsorbate separately.

The application of the DFT theory to Pt clusters has been shown to be useful in predicting the energetics for adsorption of CO and ethylene on supported Pt catalysts.[16,18,19] The distances between each of the 12 Pt atoms on the surface of the Pt_{13} cluster were constrained to be 277 pm, which is the interatomic distance for bulk Pt. The Pt−C and C−O distances for CO adsorbed at atop and bridge-bonded sites were constrained to the values determined from full geometry optimizations of CO adsorbed on 10-atom Pt clusters.[18] We note the limitations of this cluster approach to predict the energetics of CO adsorption, in view of the effects of the structure and size of the Pt cluster. Nevertheless, the relative differences between the adsorption energies for different adsorbate arrangements should be useful in predicting the proper energetic trends.

3e. Monte Carlo Simulation. The model employed in our Monte Carlo (MC) simulation was a hexagonal, two-dimensional, 42×42 lattice with periodic boundary conditions. This hexagonal lattice was chosen to represent a Pt(111) surface, since Pt particles on weakly interacting supports are expected to have mainly Pt(111) morphology. In addition, other low-index planes are known to reconstruct during CO adsorption because of strong surface−adsorbate interactions (e.g. ref 9). The size of the lattice was chosen on the basis of results reported in the literature for simulations of adsorption processes on metal surfaces.[20,21]

The MC simulation is based on the grand canonical ensemble, for which the chemical potential and temperature are specified. In this work, the chemical potential of the species adsorbed on the lattice is set equal to that of the gas-phase adsorbate. The chemical potential of the adsorbate in the gas is determined by assuming ideal gas behavior for a given pressure and temperature. The trial moves, acceptance criteria, and the overall simulation algorithm are described elsewhere (e.g. ref 22). The formation of the two types of surface species is accounted for by considering the gas phase to be a mixture of two hypothetical

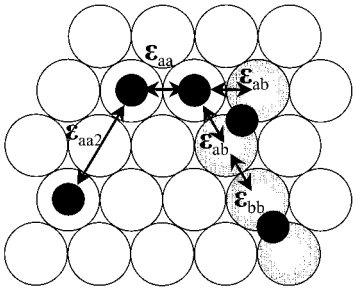

Figure 1. Pairwise interactions between adsorbed species in the MC model: (1) ϵ_{aa}, interaction between two nearest-neighbor atop-bonded species; (2) ϵ_{aa2}, interaction between two next-nearest-neighbor atop-bonded species; (3) ϵ_{bb}, interaction between two neighboring bridge-bonded species; (4) ϵ_{ab}, interaction between neighboring atop and bridge-bonded species. Interactions of a bridge-bonded CO are counted for each of the two Pt atoms associated with it. These atoms are shown as shaded.

gases: one species that forms atop-bonded CO on the lattice and the other species that forms bridge-bonded CO. The two hypothetical gases in the mixture have identical chemical potentials.

The MC simulation uses six interaction parameters to describe the energetics of CO adsorption on the model Pt(111) surface. The first parameter, atop−Pt, ϵ_a, corresponds to the negative change in potential energy of the system caused by the formation of an atop species on a clean surface. The second parameter, bridged−Pt, ϵ_b, is a similar parameter that corresponds to the formation of a bridge-bonded species on a clean surface.

To account for the decrease in the heat of adsorption with coverage, four additive and invariant pairwise repulsive interaction parameters between adsorbed species on the lattice are considered. A diagram of all pairwise repulsive interactions for a sample arrangement of adsorbed molecules is shown in Figure 1. The first pairwise repulsion parameter, atop−atop, ϵ_{aa}, represents the repulsion between two neighboring atop species on the lattice. The second repulsion parameter, atop−next neighbor, ϵ_{aa2}, represents the repulsion between two atop species at next-nearest-neighbor sites. The positions of the six nearest neighbor and twelve next-nearest-neighbor sites for a given atop site are shown in Figure 2a. The atop−atop and atop−next neighbor parameters reduce the energy of interaction at an atop site by the number of nearest and second neighbor Pt sites occupied by other atop molecules times the value of the corresponding repulsion parameter ($\epsilon_a - N_{\text{neighbors}} \times \epsilon_{aa} - N_{\text{next-neighbors}} \times \epsilon_{aa2}$). The next-nearest-neighbor repulsion, ϵ_{aa2}, for the atop species was introduced on the basis of the reported calorimetric results showing a decrease in the heat of CO adsorption on Pt(111) at low coverage.[1] Another possible explanation for the observed initial decrease in the heat of adsorption at low coverage is preferential adsorption of CO on a small number of non-Pt(111) sites.[23]

The third repulsive interaction, bridged−bridged repulsion, ϵ_{bb}, represents the repulsion between two neighboring bridge-bonded species on the lattice. For evaluation of the effect of this repulsive interaction, the eight neighboring sites of a molecule adsorbed in the bridge-bonded position are analyzed according to the diagram shown in Figure 2b. The pairwise repulsions are counted for each of the two Pt atoms associated with the bridge-bonded CO. These two atoms are shown as shaded in Figure 2b. The neighbor sites of the first atom associated with the bridge-bonded CO have labels 1, 2, 3, 7, and 8. The neighbor sites of the second atom have labels 3, 4, 5, 6, and 7. Therefore, the pairwise repulsions for the atoms with labels 3 and 7, which are neighbors of both bridge-bonded CO Pt atoms, are counted twice. Accordingly, if Pt atoms labeled 3 or 7 are associated with another bridge-bonded molecule, then the interaction energy is decreased by two times the bridged−bridged repulsion parameter ($\epsilon_b - 2\epsilon_{bb}$) for the considered molecule. Sharing of a Pt atom by two bridge-bonded CO molecules was not allowed in the MC model, because such configuration is believed to be energetically unfavorable.

The last repulsion interaction, atop−bridged, ϵ_{ab}, represents the repulsion between an atop and a bridge-bonded species on the lattice. For an atop molecule, the six neighboring metal atoms are analyzed. These are the same six neighbors that are analyzed for the atop−atop parameter. The interaction energy is modified by the atop−bridged parameter times the number of these six neighbors associated with bridge-bonded species ($\epsilon_a - N_{\text{neighbors}} \times \epsilon_{ab}$). For a bridge-bonded molecule, the eight neighboring sites shown in Figure 2b are analyzed. The interactions are counted for each of the two Pt atoms associated with the bridge-bonded CO in the same way as for the bridged−bridged repulsion, ϵ_{bb}, described above.

The MC simulation was run by specifying a temperature and then increasing the pressure in exponential steps from a small value, which would correspond to an initial coverage of about 0.001 ML, to some final value, after which further increases did not produce measurable changes in the lattice coverage or energy. The logarithmic scale for the pressure steps was used because it gives a smooth increase in coverage with increasing pressure. The first pressure calculation started with a clean surface, and each consecutive step proceeded using as a starting point the lattice configuration and the total energy determined during the previous step.

Fluctuations in the values of the lattice coverage, energy, and ratio of bridge-bonded species were monitored to determine simulation convergence. A typical number of trials to reach

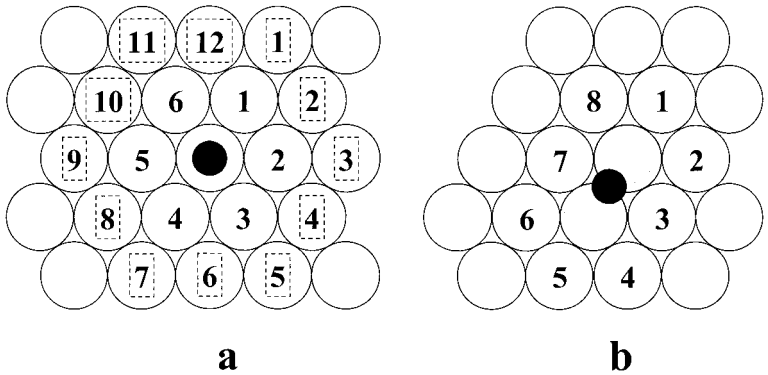

Figure 2. Positions of neighbor sites on a hexagonal lattice: (a) nearest-neighbor (1−6) and next-nearest-neighbor (1−12) sites for an atop-bonded species; (b) nearest-neighbor sites for a bridge-bonded species.

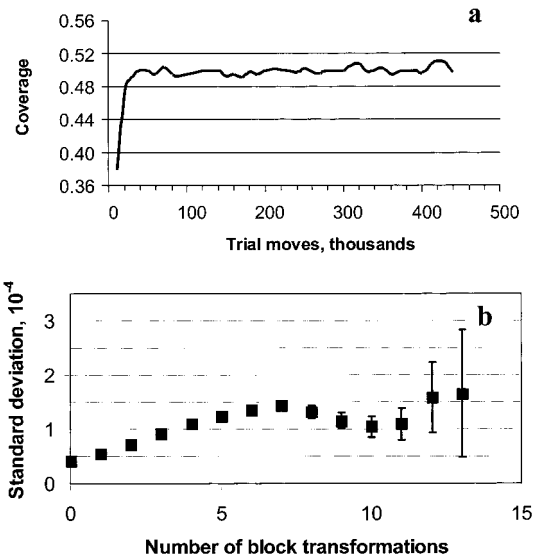

Figure 3. (a) Lattice partial coverage as a function of simulation time at 2 Torr and 673 K. (b) Estimate for the coverage standard deviation at 2 Torr and 673 K obtained with the block transformation method.[24] The estimate remains constant at ca. 1.1×10^{-4} after 9, 10, and 11 block transformations.

equilibration was $(2-5) \times 10^4$ for the coverage range from 0 to 0.5. A plot of the partial lattice coverage versus the number of trials at 2 Torr and 673 K, which is typical for this coverage range, is shown in Figure 3a. The average coverage at these conditions is 0.50084 ± 0.00022, and the equilibration is reached after about 5×10^4 trial moves. The standard deviations of the monitored values as well the convergence of the simulation runs were determined by the block transformation method of Flyvbjerg and Petersen.[24] The first 10^6 trial moves were used to allow the system to equilibrate, and these initial results were discarded. After the equilibration, 16 384 (2^{14}) data points were collected by averaging results of 1000 individual consecutive trial moves for each data point. Thus, the total number of trial moves was 1.7×10^7. The 16 384 data points were analyzed by block transformations. The dependence of the estimate for the coverage standard deviation at 2 Torr and 673 K on the number of block transformations is shown in Figure 3b. After 9, 10, and 11 block transformations, the estimate remains constant at ca. 0.00011, indicating that the individual points are no longer correlated and this is a reasonable estimate. All values for coverages up to 0.5 were obtained by following this algorithm, i.e., equilibration for 10^6 trial moves followed by collection of 16 384 points by averaging results of 1000 consecutive moves for each point and taking the estimate of the standard deviation after 11 block transformations. For coverages exceeding 0.5, fluctuations in monitored values were analyzed in a similar way. For this high coverage range, the equilibration time was extended to 10^8 trial moves, and the 16 384 points for the error analysis were collected by averaging results of 40 000 individual consecutive moves for each point. Estimates of standard deviations were again obtained after 11 block transformations on the basis of the analysis of the dependency of the estimates on the number of transformations.

The differential energy of adsorption from the MC simulation was calculated by subtracting the energy of the system before a pressure increase from the energy after the pressure increase. This energy difference was then divided by the number of moles adsorbed during the pressure increase. The energy of adsorption was adjusted by $3/2kT$ to obtain the adsorption enthalpy, thereby accounting for the loss of the translational energy of gaseous CO during adsorption. The error estimates for differential energy values were calculated similarly to the estimates for other values by generating and analyzing 16 384 points by block transformations. The estimates of standard deviations were similarly obtained after 11 block transformations.

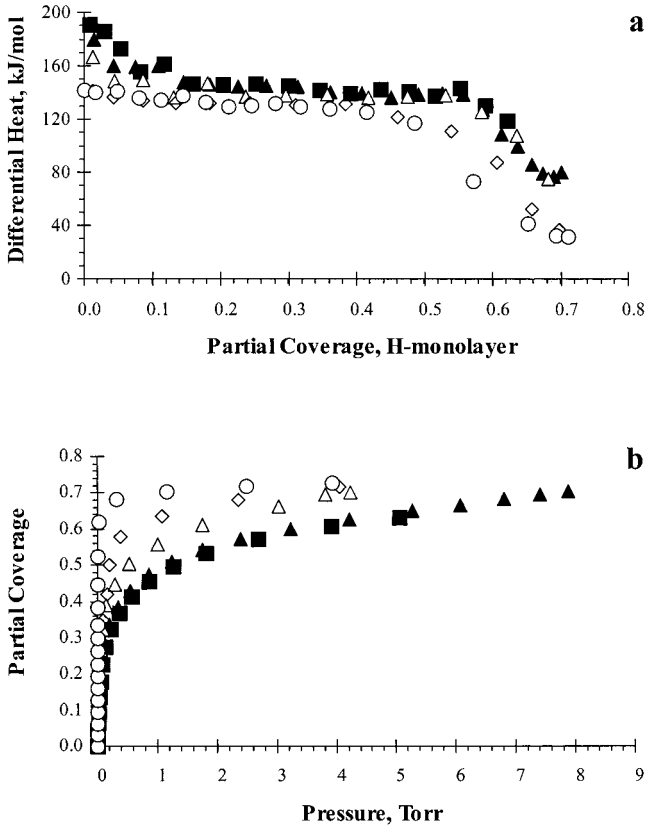

Figure 4. (a) Differential heats and (b) adsorption isotherms for CO adsorption on Pt/SiO_2 at 298 K (○), 473 K (◇), 573 K (△), and 673 K (■, run 1; ▲, run 2).

4. Results

4a. Microcalorimetric Results. Microcalorimetric experiments were performed at 298, 473, 573, and 673 K. Plots of differential heat versus CO coverage and the corresponding normalized adsorption isotherms are presented in Figure 4a,b. At room temperature, the initial heat of CO adsorption on Pt/SiO_2 is about 140 kJ/mol. The value of the differential heat of adsorption decreases to 120 kJ/mol at a normalized CO coverage of 0.5 ML. As the coverage increases above 0.5, the heat of adsorption decreases to about 30 kJ/mol at a coverage of 0.7. The sharp decrease in the heat of adsorption at coverages approaching the saturation coverage of CO can be attributed to the simultaneous adsorption of CO on Pt and on the silica support, leading to an average heat. At temperatures of 573 K and higher, the adsorption on silica becomes negligible at our experimental pressures, and the differential heat declines with coverage to a limiting value of 75 kJ/mol, which can be attributed to the heat of CO adsorption on Pt at saturation coverage.

The plot of differential heat versus CO coverage at 473 K is similar to the microcalorimetric results obtained at room temperature. These microcalorimetric and volumetric data at 298 and 473 K for the Pt/SiO_2 catalyst used in this study are in agreement with published results for CO adsorption on Pt/SiO_2 and Pt/L-zeolite at 403 K.[25] At 573 K, the initial heat of CO adsorption on Pt/SiO_2 increases to 167 kJ/mol, which is in agreement with the reported value of 175 kJ/mol for CO

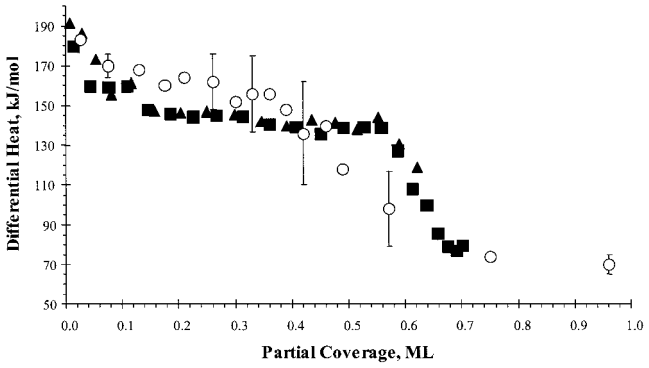

Figure 5. Comparison of CO heats of adsorption on Pt/SiO_2 at 673 K (■, run 1; ▲, run 2) and on Pt(111) at 300 K (○). The error bars for the Pt(111) data indicate standard deviations for six runs.[1]

adsorption on Pt/L-zeolite at that temperature.[18] As the temperature is increased to 673 K, the initial heat of CO adsorption on Pt/SiO_2 increases to 180−190 kJ/mol. This range of heats is in agreement with the value of 183 ± 8 kJ/mol reported for the initial heat of CO adsorption on Pt(111).[1] A comparison is provided in Figure 5 between our microcalorimetric results at 673 K and data for Pt(111) at 300 K.[1] This figure shows agreement in the behavior of Pt/SiO_2 and Pt(111) with respect to the initial heat of CO adsorption and also to the dependence of the heat on CO coverage.

The reproducibility of the microcalorimetric data was tested by performing two series of measurements at 673 K, and these data are presented in Figures 4 and 5. With the exception of the initial heats that were different by 10 kJ/mol, the heat of adsorption data for the two series of measurements were within 5 kJ/mol. After the second series of microcalorimetric measurements at 673 K, the dispersion of the catalyst was lower by 4% (i.e., 58% compared to 62% for the first series), as determined by hydrogen adsorption. However, after normalization by the appropriate saturated hydrogen coverage, the CO adsorption isotherms in terms of fractional CO coverage were essentially identical (Figure 4b).

After each series of microcalorimetric measurements at 473, 573, and 673 K, the cells were evacuated overnight at the measurement temperature to a dynamic pressure of 10^{-7} Torr. The total amount of heat consumed by CO desorption was determined, from which the total amount of desorbed CO was estimated. The ratio of the amount of desorbed CO to the amount of CO adsorbed at saturation coverage is an indication of the reversibility of the CO adsorption process at each temperature. This ratio was equal to 0.98 and 0.95 at 673 K (for the two series of experiments described above), 0.69 at 573 K, and 0.42 at 473 K. These ratios show that essentially all adsorbed CO species desorb from the catalyst at 673 K; therefore, CO adsorption on Pt/SiO_2 is equilibrated at 673 K. This behavior is in agreement with TPD data reported for a Pt(111) single crystal,[6] a polycrystalline Pt foil,[26] and supported Pt catalysts.[27] At temperatures below 673 K, desorption of CO is not complete for the times of the present study (i.e., 12 h), indicating that CO adsorption at these temperatures is not completely equilibrated.

Finally, at the temperatures of the present study, the CO adsorption isotherms approach a saturation coverage of about 0.7 ML (Figure 4b), and this value agrees with data reported for Pt(111) surfaces and supported Pt catalysts.[2,4,9,10,28]

4b. FTIR Results. Figure 6 presents FTIR spectra obtained by sequentially dosing CO onto Pt/SiO_2 at room temperature. The first two spectra for apparent CO coverages of 0.1 and 0.2

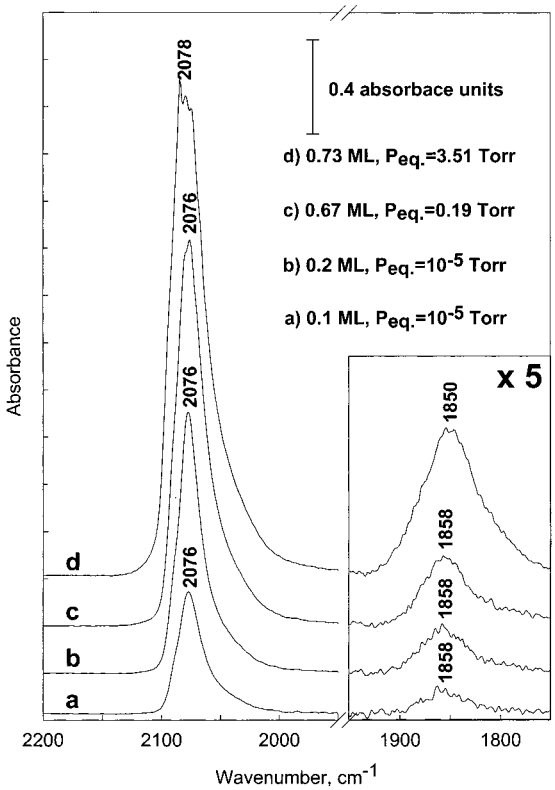

Figure 6. FTIR spectra of CO adsorbed on Pt/SiO_2 at 298 K; sequential dosing.

ML were obtained by dosing a known amount of CO onto the pellet, based on the total number of surface Pt atoms determined from the pellet mass. The residual CO pressure in the IR cell after dosing was on the order of 10^{-5} Torr. The CO coverages of 0.67 and 0.73 ML were achieved using CO pressures of 0.19 and 3.51 Torr, respectively, as determined from the room temperature adsorption isotherm in Figure 4b. All features of the spectra at different CO coverages are essentially identical, i.e., the relative intensities of the two peaks and the positions of their maxima are constant, and only the total absorbance increases with coverage. These spectra are in agreement with results reported for other supported Pt catalysts.[3,15] The main peak at 2076 cm^{-1} is associated with CO adsorbed in the atop position, and the weaker, broader peak at 1858 cm^{-1} is associated with bridge-bonded CO. The band positions at saturation CO coverage are 2078 cm^{-1} for the atop and 1850 cm^{-1} for the bridge-bonded species.

Figure 7 shows IR spectra at 673 K for various CO pressures. The CO coverages indicated in this figure were estimated from the adsorption isotherm at 673 K in Figure 4b. At low CO coverage, the bands from atop and bridge-bonded CO are located at 2054 and 1864 cm^{-1}, and these positions are in agreement with literature data for Pt(111).[3] The position of the atop band shifts to high wavenumbers with increasing coverage, changing from 2054 cm^{-1} at 0.4 ML to 2064 cm^{-1} at saturation coverage. This behavior is also in agreement with data for CO on Pt(111). The position of the band for bridge-bonded CO does not change significantly with coverage (1864 − 1856 cm^{-1}), while the half-width of this band increases with coverage. It should be noted that bands near 2350 cm^{-1} were detected at CO pressures higher than 12 Torr, which can be attributed to the formation of gaseous CO_2 from the disproportionation of CO, i.e., $2CO \rightarrow CO_2 + C$. After this series of IR spectra at 673 K, the infrared cell was sealed, cooled to room temperature, and an IR spectrum was collected (see Figure 7).

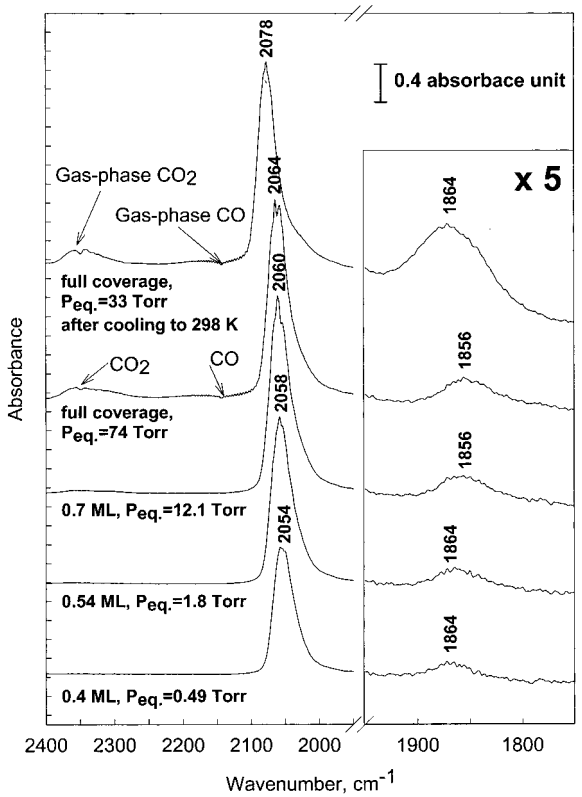

Figure 7. FTIR Spectra of CO adsorbed on Pt/SiO_2 at 673 K; sequential dosing.

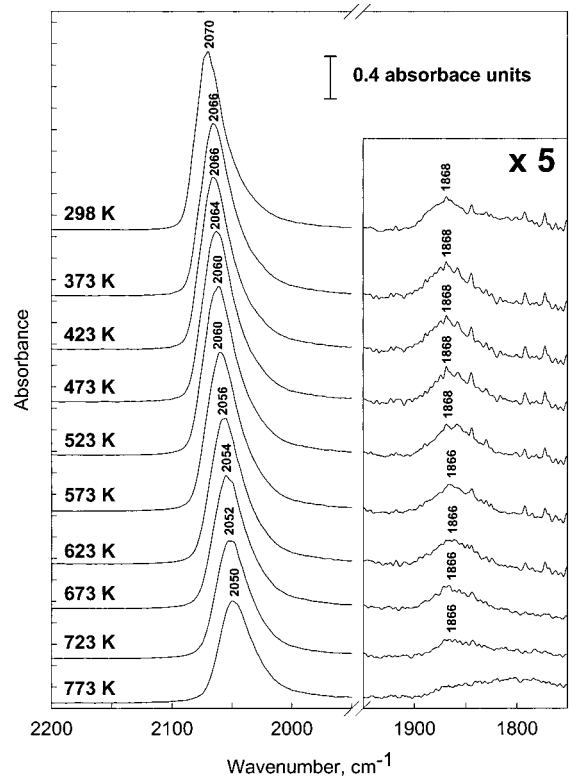

Figure 8. FTIR spectra of CO adsorbed on Pt/SiO_2; isobaric cooling from 773 to 298 K at 0.4 Torr of CO.

Figure 8 shows a series of IR spectra collected at different temperatures for a CO isobar at 0.4 Torr, starting at 773 K and cooling to 298 K. Initially, at the highest temperature of 773 K, bridge-bonded CO species were not observed. This behavior is in agreement with the preferential occupation of atop sites at low CO coverage in equilibrated, single-crystal experiments. Decreasing the temperature from 773 K to room temperature causes a shift of the atop band from 2050 to 2070 cm^{-1}. The position of the bridge-bonded band remained constant at 1866−1868 cm^{-1}. This same series of IR experiments was conducted for a CO isobar at 10 Torr, and the positions of the bands for the atop and bridge-bonded CO at 773 K were 2060 and 1864 cm^{-1}. All trends with temperature shown in Figure 8 at 0.4 Torr were also observed for the isobar at 10 Torr. After cooling to room temperature at 10 Torr, the IR spectrum obtained was essentially the same as the spectrum obtained by sequential dosing of CO to saturation coverage at room temperature, and both of these spectra are similar to the spectrum collected after dosing CO to saturation coverage at 673 K followed by cooling to room temperature.

TABLE 1: Ratio of Integrated Absorbances of Bridge-Bonded to Atop CO

sequential dosing							
298 K		673 K		0.4-Torr isobar		10-Torr isobar	
θ, ML	ratio	θ, ML	ratio	T, K	ratio	T, K	ratio
0.1	0.061	0.4	0.021	773	0.000	673	0.046
0.2	0.071	0.5	0.032	723	0.037	623	0.050
0.67	0.082	0.7	0.043	673	0.052	573	0.056
0.71	0.118			623	0.055	573	0.054
				573	0.060	523	0.059
				523	0.059	473	0.071
				473	0.062	473	0.077
				423	0.069	423	0.094
				373	0.083	373	0.101
				298	0.094	298	0.128

TABLE 2: DFT Calculation Results

DFT models	$-\Delta E_{ads}$, kJ/mol
atop	217
second atop−para	201
second atop−ortho	189
bridge-bonded	193
bridge-bonded as a neighbor of atop	190
two bridge-bonded as neighbors	196

The absorbance ratio of bridge-bonded to atop CO is shown in Table 1 as a function of CO coverage for the spectra at 298 K of Figure 6 and for the spectra at 673 K of Figure 7. In addition, the ratio is shown as a function of temperature for the isobar spectra at 0.4 Torr of Figure 8 and isobar spectra at 10 Torr. To verify the equilibration of CO during the isobaric cooling, the pellet was reheated to 773 K and then cooled again twice to 573 and 473 K. The spectra before and after the reheating were essentially identical, with similar absorbance ratios as shown in Table 1. With decreasing temperature from 773 to 298 K in the CO isobar experiments, the absorbance ratio of bridge-bonded to atop CO increased from 0 to 0.09 for the isobar at 0.4 Torr, and the ratio increased to 0.12 for the isobar at 10 Torr. For the spectra at 673 K, the absorbance ratio increases from 0.02 to 0.04 with increasing CO coverage from 0.4 ML to saturation coverage at 673 K. On the other hand, at room temperature, this ratio is constant and equal to 0.07−0.08 as the apparent coverage increases from 0.1 to 0.67 ML. At saturation coverage, the ratio increases to 0.12.

4c. DFT Calculation Results. Changes in electronic energies for several modes of adsorbed CO on Pt_{13} clusters were calculated to estimate the strengths of bonding for CO at atop and bridge-bonded sites and to estimate the values for lateral repulsion parameters. The results of the DFT calculations are summarized in Table 2. The estimates for the MC parameters obtained from these results are shown in Table 3. The energy

TABLE 3: DFT Estimates and Fitted Values for the MC Simulation Parameters

MC parameters	DFT estimates, kJ/mol	fitted MC values, kJ/mol
atop−Pt, ϵ_a	217	170
bridged−Pt, ϵ_b	193	140
atop−atop, ϵ_{aa}	28	18
atop−atop next neighbor, ϵ_{aa2}	16	6
bridged−bridged, ϵ_{bb}	−1.5	0
atop−bridged, ϵ_{ab}	1.5	0

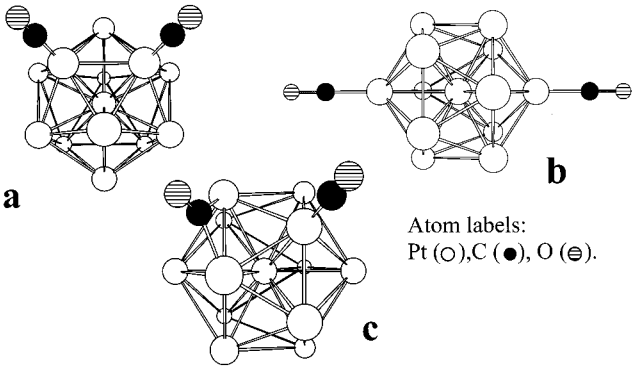

Figure 9. Models of a Pt_{13} cluster with two adsorbed CO molecules: (a) on atop sites in the ortho configuration, (b) on atop sites in the para configuration, (c) on atop and bridge-bonded sites in the nearest-neighbor configuration.

change for adsorption of CO at atop sites was estimated to be 217 kJ/mol, while the energy change for formation of bridge-bonded CO is lower by 24 kJ/mol. The lower initial heat of adsorption for bridge-bonded CO species is in agreement with the preferential formation of atop species at low coverage in single-crystal experiments and in our FTIR spectra for low CO coverages at 773 K. When the Pt_{13} cluster contains one adsorbed CO molecule at an atop site, the addition of a second atop CO at a nearest-neighbor position results in a decrease in the energy of adsorption by 28 kJ/mol. The geometry of the Pt_{13} cluster model with two atop-bonded CO species at nearest-neighbor sites is shown in Figure 9a. The addition of the second atop CO at a next-nearest-neighbor position, as shown in Figure 9b, decreases the energy of adsorption by 16 kJ/mol. When the Pt_{13} cluster contains one adsorbed CO molecule at an atop site, the addition of a second CO molecule at a neighboring bridge-bonded site, as shown in Figure 9c, results in a decrease in the energy of adsorption by 3 kJ/mol. This change corresponds to two atop−bridged repulsion interactions of 1.5 kJ/mol. Finally, when the Pt_{13} cluster contains one adsorbed CO molecule at a bridge-bonded position, the addition of a second CO molecule at a neighboring bridge-bonded position results in a slight increase in the energy of adsorption by 3 kJ/mol. This result was used as an indication that the bridged−bridged repulsion parameter in the MC simulation should be very small.

4d. Monte Carlo Simulation Results. The energetic parameters of the MC simulation were adjusted to fit our experimental data of differential heat versus CO coverage and the corresponding isotherm for the equilibrated adsorption of CO on Pt/SiO_2 at 673 K and to fit the experimental data of differential heat versus CO coverage for the equilibrated adsorption of CO on Pt(111) at 300 K.[1] The results from our DFT calculations were used to provide initial estimates for the energetic parameters. When the DFT results were used directly in the MC simulations, the qualitative results were similar to our final fits, but the differential heat curves were shifted by about 50 kJ/mol compared to the experimental data.

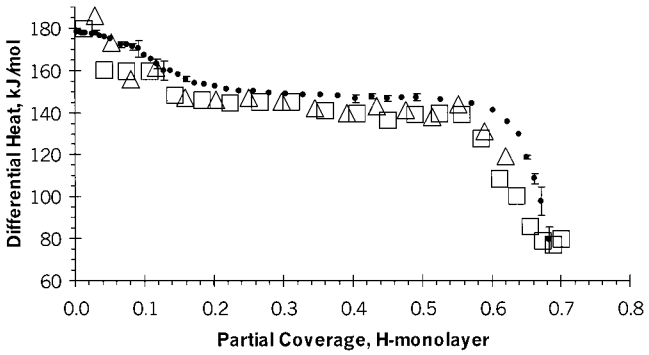

Figure 10. Comparison of experimental differential heats of CO adsorption on Pt/SiO_2 at 673 K (□, run 1; △, run 2) with MC simulation results at the same temperature (●).

Table 3 presents a summary of the fitted MC simulation parameters and the initial estimates of these parameters from DFT calculations. The potential energy change associated with the formation of an atop CO species on a clean Pt surface is predicted to be 170 kJ/mol. With the correction for $3/2kT$ at 673 K, this value corresponds to the initial heat of CO adsorption of 178 kJ/mol. The fitted values for the second and nearest-neighbor repulsion parameters for the atop species are 6 and 18 kJ/mol, respectively. These values are consistent with the DFT predictions of 16 and 28 kJ/mol for these repulsive interactions. The fitted value for the potential energy change associated with the formation a bridge-bonded CO species is 140 kJ/mol. This value corresponds to a difference of 30 kJ/mol between the initial heats of adsorption of the atop and bridge-bonded species, and this difference is in agreement with the DFT predictions. The fitted values of the atop−bridged and bridged−bridged repulsion parameters are zero, and these values are also in good agreement with the DFT predictions. In addition, these zero values reduce the number of energetic parameters used in the MC simulation model to four: the heats of formation of atop− and bridge-bonded species on a clean lattice and two pairwise repulsive interactions between atop−bound molecules.

Figures 10 and 11a show comparisons of the MC simulation results with the experimental plot of differential heat versus coverage on Pt/SiO_2 and the corresponding adsorption isotherm at 673 K. The calculated fraction of adsorbed CO present as bridge-bonded species is shown in Figure 11b as a function of total surface coverage at 673 K. Error bars for the calculated values denote confidence intervals of four standard errors. The error bars are shown only if these intervals are larger than the size of the plot symbols.

The initial heat of adsorption corresponds to the formation of exclusively atop species. As the coverage increases, the heat decreases because of the next-nearest-neighbor atop−atop repulsion, ϵ_{aa2}. The heat of adsorption approaches a constant value of about 145 kJ/mol at a coverage of 0.2. In the coverage range from 0.2 to 0.5 ML, CO populates both atop and bridge-bonded sites, since the values of the bridged−bridged, ϵ_{bb}, and atop−bridged, ϵ_{ab}, interactions are close to zero. As the coverage exceeds half of the monolayer, the adsorption of CO leads to occupation of adjacent atop sites. Because of the additional atop−atop repulsive interaction, ϵ_{aa}, the heat of adsorption decreases to about 75 kJ/mol at saturation coverage. At the coverage of 0.7 ML, the atop species occupy 40% of all Pt sites and the bridge-bonded species occupy the other 60%. The repulsion interactions at a coverage of 0.7 ML are balanced such that the heats of adsorption of two atop species and one bridge-bonded species are almost equal.

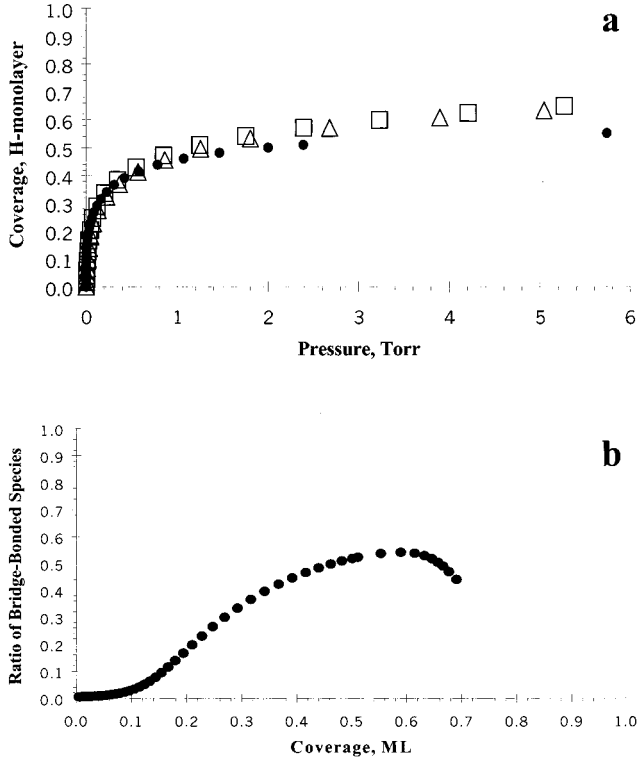

Figure 11. (a) Comparison of experimental isotherms for CO adsorption on Pt/SiO_2 at 673 K (□, run 1; △, run 2) with MC simulation results at the same temperature (●); (b) Ratio of bridge-bonded species as a function of total coverage predicted by the MC simulation at 673 K.

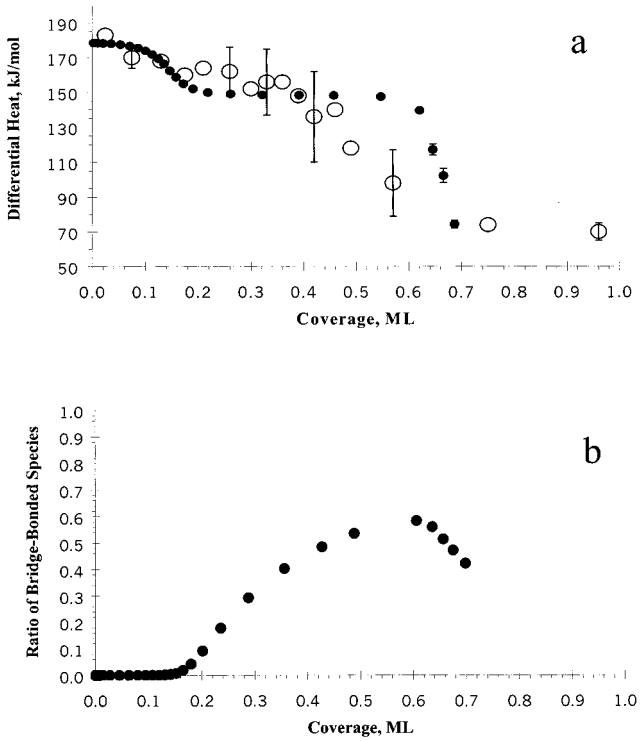

Figure 12. (a) Comparison of differential heats of CO adsorption on Pt(111) at 300 K from ref 1 (○) with MC simulation results at the same temperature (●); (b) Ratio of bridge-bonded species as a function of total coverage predicted by the MC simulation at 300 K.

Figure 12a presents a comparison of the MC simulation results with the experimental calorimetric results at various coverages for CO adsorption on Pt(111) at 300 K.[1] The calculated fraction of the adsorbed CO present as bridge-bonded species at 300 K is shown in Figure 12b. It can be seen that the results of the MC simulations with the same interaction parameters that we employed to describe our data for Pt/SiO_2 at 673 K are in general agreement with the calorimetric data for Pt(111). At 300 K, the dependence on coverage of the fraction of bridge-bonded CO species (Figure 12b) is similar to the behavior at 673 K (Figure 11b), i.e., the atop species are formed first, followed by the population of bridge-bonded species, and then finished predominantly by the occupation of atop sites. When the difference in the heats of adsorption of atop and bridge-bonded species is small compared to kT, formation of both species is likely (e.g., at 673 K). With decreasing temperature, however, the small energetic differences between the atop and bridge-bonded species become more important, as evidenced by the higher initial occupation of only atop sites at 300 K, the more rapid increase in the fraction of bridge-bonded species at coverages from 0.2 to 0.5, and the steeper decline in the fraction of bridge-bonded species at coverages exceeding half of the monolayer. This effect of temperature on the population of bridge-bonded CO has been observed experimentally.[8,12]

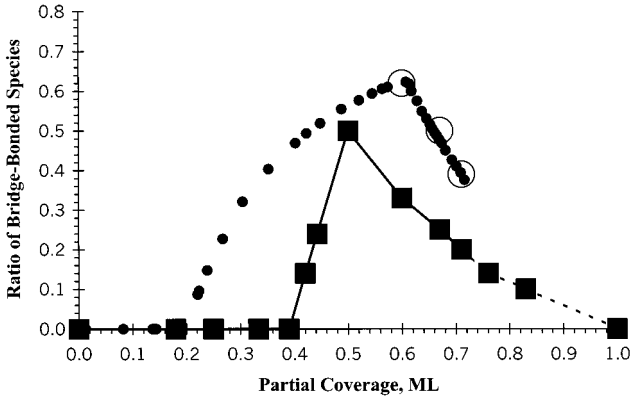

Figure 13. Ratio of bridge-bonded CO as a function of total coverage predicted by the MC simulation at 100 K (●). Results of a canonical MC simulation after slow cooling from 500 to 50 K: a full force field model (■) and lattice-gas model (○).[2]

Figure 13 shows results of MC simulations at various total coverages for the fraction of adsorbed CO present as bridge-bonded species at 100 K, and these results are compared with the modeling results reported by Persson et al.[2] for CO adsorption on Pt(111). In that study, Persson et al. used a canonical MC ensemble with a detailed force field constructed on the basis of their single-crystal spectroscopic studies. The total surface coverage in a canonical ensemble simulation is fixed, and only the positions of surface species are allowed to change in trial moves. In contrast, in a grand canonical ensemble simulation, not only the positions but also concentrations of surface species are allowed to change. A grand canonical ensemble simulation, therefore, is able to provide all the information that can be derived from a canonical ensemble and additionally a dependence of surface concentrations on the chemical potential (pressure) of the gas-phase species. Unlike our simplified model and the lattice gas approximation employed by Persson et al., their full force field accounted for the energetic differences caused by small changes in the positions of atop and bridge-bonded species relative to the bonding Pt atoms.[2] The main difference between the results of the two types of simulations, as can be seen in Figure 13, is the generally higher fraction of bridge-bonded CO predicted by the models with only symmetric surface species.

5. Discussion

Metal particles on a supported catalyst are generally present uniformly on the surface of the support, and they are not in direct contact with each other. The absence of a continuous metal surface for such a supported metal catalyst diminishes the ability of molecules adsorbed on the metal to equilibrate with each other by surface diffusion, since the strength of adsorption on the support is typically low compared to that on the metal, i.e., adsorbed molecules can equilibrate between metal particles only by desorption into the gas phase.

As determined in our microcalorimetric experiments, the heat of CO adsorption on Pt/SiO_2 in the coverage range of up to 0.6 ML is 140−180 kJ/mol. With a standard preexponential factor of 10^{13} s^{-1}, the rate constant for CO desorption at 298 K in this coverage range is from 10^{-12} to 10^{-19} s^{-1}. Therefore, the rate of CO desorption is negligible under these conditions, and the absence of desorption processes makes CO equilibration possible only over each metal particle but not between different metal particles on our Pt/SiO_2 catalyst. Accordingly, adsorption of CO on our Pt/SiO_2 catalyst at room temperature creates a distribution of coverages on our sample, i.e., most of the Pt particles are either at zero coverage or close to saturation coverage (0.6 ML), depending on whether they have been exposed to CO. Specifically, the adsorption process takes place chromatographically, where doses of carbon monoxide sequentially saturate the Pt particles that first come into contact with gaseous CO. The adsorption remains nonequilibrated until a coverage of about 0.6 ML. At this coverage, the heat of adsorption decreases to the saturation value of about 75 kJ/mol, and further adsorption of CO at 298 K to the saturation coverage of about 0.7 ML is equilibrated, since the value of the desorption rate constant becomes on the order of 1 s^{-1}.

The lack of equilibration during dosing of CO onto Pt/SiO_2 at 298 K is reflected in the IR spectra of Figure 6. These spectra at different total CO coverages are similar to the spectrum obtained at saturation coverage, and increasing the total coverage simply increases the number of Pt particles that are at essentially full coverage. After the total coverage of about 0.6, the system becomes equilibrated and further increases in total coverage lead to changes for all Pt particles. When CO adsorption becomes equilibrated with the Pt particles at these high total coverages, the extent of dipole coupling of the atop species and the ratio of bridge-bonded to atop species change with increasing coverage. Consequently, the increase in the total coverage from about 0.6 to 0.7 ML results in an increase in the wavenumber of the band from atop species (Figure 6) and a change of the absorbance ratio for bridge-bonded to atop species (Table 1). This behavior is in agreement with reports in the literature that IR spectra collected at 298 K for CO on Pt/SiO_2 at pressures of 10^{-8} Torr changed slowly over a period of several days, whereas equilibration of CO with the sample was faster at higher temperatures and pressures.[29]

The microcalorimetric results for CO adsorption on Pt/SiO_2 at room temperature also reflect the chromatographic, nonequilibrated nature of the adsorption process. Platinum particles on the support are sequentially titrated with CO, and the heat released after each dose corresponds to the average heat of adsorption for the coverage range from 0 to ca. 0.6 ML. At 573 K, the adsorption of CO becomes more equilibrated, and the observed initial heat of adsorption is higher than at room temperature (Figure 4a). Finally, at 673 K, the adsorption of CO is fully equilibrated with the Pt/SiO_2 sample, as evidenced by the ability of CO to desorb completely from the sample at this temperature. The equilibration of CO with the Pt/SiO_2 sample at 673 K is also evidenced by the similarity of the plot of differential heat versus coverage for this sample with the corresponding plot reported for Pt(111) (Figure 5).

The IR spectra collected for increasing CO coverage on Pt/SiO_2 at 673 K are in agreement with vibrational spectra reported for the equilibrated adsorption of CO on Pt(111). At this temperature, the frequency of the atop band increases with coverage (Figure 7), and the absorbance ratio of bridge-bonded to atop species changes with coverage (Table 1) until the saturation coverage is reached. The same phenomena are observed when the CO coverage is increased under equilibrium conditions by slowly cooling a catalyst pellet at constant CO pressure (Figure 8 and Table 1).

As noted above, CO adsorption at 298 K becomes equilibrated for Pt/SiO_2 at high total coverages. In addition, surface diffusion over a given metal particle leads to equilibration of adsorbed CO for that particle (similar to the situation for a single-crystal surface). This behavior explains why the IR spectra collected at 298 K for saturation CO coverage do not depend on the manner in which the sample was exposed to CO. In particular, similar IR spectra for saturation coverage are obtained by sequential dosing of CO at room temperature, by dosing at 673 K followed by cooling to room temperature, and by cooling from 773 K to room temperature at a constant CO pressure of 10 Torr. Moreover, these spectra are similar to the vibrational spectra reported at saturation coverage for Pt single-crystals and foils at 298 K.

The results of CO adsorption on our Pt/SiO_2 are important in view of the wide use of CO for characterization of supported metal catalysts. The use of CO as a probe is based on several approaches. The first approach is to use the CO saturation coverage obtained by volumetric titration as an estimate of the number of accessible Pt atoms.[4,30] The results of our MC simulations and volumetric measurements of the extent of CO adsorption on Pt/SiO_2 suggest that temperature and method of titration have a small effect on the total CO coverage and on the ratio of bridge-bonded to atop species at saturation coverage. The MC simulation predicts that the ratio of bridge-bonded species to the total amount of adsorbed CO at saturation coverage is equal to $3/7 = 0.43$ for the temperature range from 300 to 673 K (Figures 11b and 12b). The experimental adsorption isotherms at different temperatures approach the same saturation limit of ∼0.7 ML (Figure 4b) and the full coverage spectra obtained with different titration methods are similar. Another approach in the use of CO to characterize catalysts is to use the CO/H ratio determined from measurements of the saturation extents of CO and H_2 adsorption as a probe of the metal surface.[25,28,31] Our results indicate that the saturation CO/H ratio should be equal to 0.7 for silica-supported Pt particles that possess the surface properties of Pt(111). Therefore, if the CO/H ratio is not equal to 0.7, then the surface adsorptive properties of Pt have been altered from Pt(111), for example, by particle-size effects, interactions with the support, or formation of surface alloys.

Another method for the use of CO adsorption for characterization of supported-metal catalysts is based on analyses of CO vibrational spectra. For example, the frequency of the band for CO on atop sites in the limit of zero coverage has been shown to depend on the electronic state of Pt atoms and, to a lesser extent, on the dispersion of Pt particles on the support.[27] Since the lack of CO equilibration with supported Pt catalysts at room temperature and low total coverages leads to IR spectra that are representative of CO adsorption at high local coverage, we note that the nonequilibration issue has to be specifically

addressed when the frequency in the limit of low coverage is evaluated. Methods for achieving CO−Pt equilibration have been recently summarized by de Menorval et al.[27] These methods are (1) isotope dilution (e.g., ref 13), (2) adsorption at room temperature followed by desorption at elevated temperatures, and (3) adsorption of small amounts at an elevated temperature followed a slow temperature decrease. In addition, the authors have proposed a hydrogen preadsorption technique: when hydrogen is preadsorbed, carbon monoxide slowly displaces it on the surface, and all Pt particles are expected to have similar total CO coverage. [27] Local CO coverage may be higher than the average total coverage due to segregation of carbon monoxide and hydrogen on the surface.[32,33]

Similar surface−adsorbate equilibration considerations should apply to the determination of the frequency shift with coverage of the atop peak. This frequency shift depends on the extent of the dipole coupling between the atop species at saturation coverage, and it is a useful indicator of the size of Pt ensembles. An estimation of dipole coupling effects as a function of metal dispersion for a series of Pt/Al_2O_3 catalysts can be found in ref 27. The absorbance of the atop peak at saturation coverage is another useful characteristic. In particular, since the ratio of bridge-bonded to atop species for CO adsorption at saturation coverage on Pt/SiO_2 is independent of the method used to dose CO onto the sample, it is possible to use the absorbance of the atop-bonded species for the estimation of the total number of accessible Pt sites.[31] We note, however, that this approach must be used with caution, as it is based on the assumption of similar dipole coupling effects for catalysts with different Pt particle sizes. While the extent of dipole coupling between atop species at saturation coverage can be expected to be similar for catalysts with low dispersions, the effects of dipole coupling may be different for catalysts with high Pt dispersions or for metal alloy catalysts.

The results of MC simulations predict that the ratio of bridge-bonded to atop species should be close to unity at a CO coverage of about 0.5 ML; however, the experimentally observed absorbance ratio of bridge-bonded to atop species is rather small for our Pt/SiO_2 catalyst at all coverages and temperatures (Table 1). First, we note that the effects of dipole coupling between atop species at high coverages lead to an increase in the apparent extinction coefficient for these species. Second, we note that the intensity of the band for bridge-bonded species is expected to be weaker for CO adsorption on a supported Pt catalyst, because of non-Pt(111) and defect sites that lead to a broadening of this band. Furthermore, the atop and bridge-bonded CO species move to slightly less symmetric positions at higher temperatures, and this loss of symmetry leads to a broadening and weakening of the absorbance band from bridge-bonded species.

The MC simulation of the present study uses a Pt(111) adsorption model based on simplified CO energetics. This simple MC simulation appears to be sufficient to describe CO adsorption data collected for a wide range of experimental conditions. In addition, this simulation can be used to consolidate experimental data collected on Pt single-crystals at low temperatures with experimental data obtained for supported Pt catalysts at elevated temperatures.

6. Conclusions

The adsorption of CO on Pt/SiO_2 is not equilibrated at temperatures below about 600 K, because the rate of CO desorption into the gas phase is negligible at these temperatures. Nonequilibrated adsorption of CO leads to sequential (chromatographic) rather than uniform population of the adsorption sites, and the measured heat of adsorption represents an average value characteristic of the coverage range from zero to a value close to the saturation coverage, at which the rate of desorption becomes appreciable. Accordingly, the heat of adsorption and the features of the IR spectra for adsorbed CO do not change significantly with increasing apparent coverage.

The adsorption of CO on Pt/SiO_2 becomes equilibrated at 673 K. At this temperature, the microcalorimetric and IR spectroscopic results obtained for Pt/SiO_2 are in agreement with literature data for equilibrated adsorption of CO on Pt(111) single crystals. The heat of adsorption at 673 K decreases with coverage from the initial value of 190−180 to 75 kJ/mol at the saturation CO coverage of 0.7 ML. In addition, the positions and intensity ratios of IR bands for atop and bridge-bonded CO change with increasing CO coverage. Similar trends are observed for spectra collected under equilibrated isobaric cooling conditions.

A simple MC simulation can be used to consolidate experimental data for equilibrated CO adsorption on our supported Pt/SiO_2 catalyst at elevated temperatures and on Pt(111) at low temperatures. Quantum chemical calculations employing DFT theory for 13-atom Pt clusters are useful for the estimation of energetic parameters employed in these MC simulations. The results from MC simulations of our experimental data suggest that the saturation coverage for CO adsorption on our Pt/SiO_2 catalyst is 0.7 ML, and this value is in agreement with the saturation coverage reported for CO adsorption on Pt(111) surfaces.

Acknowledgment. Acknowledgment is made to the donors of the Petroleum Research Fund, administered by the American Chemical Society, for support of this research. We also thank Dr. Qiliang Yan for valuable discussions about MC simulations.

References and Notes

(1) Yeo, Y. Y.; Vattuone, L.; King, D. A. *J. Chem. Phys.* **1997**, *106*, 392.

(2) Persson, B. N. J.; Tushaus, M.; Bradshaw, A. M. *J. Chem. Phys.* **1990**, *92*, 5034.

(3) De La Cruz, C.; Sheppard, N. *Spectrochim. Acta A* **1994**, *50*, 271.

(4) Jackson, S. D.; Glanville, B. M.; Willis, J.; McLellan, G. D.; Webb, G.; Moyes, R. B.; Simpson, S.; Wells, P. B.; Whyman, R. *J. Catal.* **1993**, *139*, 207.

(5) Nekrylova, J. V.; Harrison, I. *J. Chem. Phys.* **1996**, *205*, 37.

(6) Steininger, H.; Lehwald, S.; Ibah, H. *Surf. Sci.* **1982**, *123*, 264.

(7) Hayden, B. E.; Bradshaw, A. M. *Surf. Sci.* **1983**, *125*, 787.

(8) Schweizer, E.; Persson, B. N. J.; Tushaus, M.; Hoge, D.; Bradshaw, A. M. *Surf. Sci.* **1989**, *213*, 49.

(9) Crossley, A.; King, D. A. *Surf. Sci.* **1980**, *95*, 131.

(10) Liu, J.; Xu, M.; Nordmeyer, T.; Zaera, F. *J. Phys. Chem.* **1995**, *99*, 6167.

(11) Hollins, P. *Surf. Sci. Rep.* **1992**, *16*, 51.

(12) Tushaus, M.; Schweizer, E.; Hollins, P.; Bradshaw, A. M. *J. Electron Spectrosc. Relat. Phenom.* **1987**, *44*, 305.

(13) Fox, S. G.; Browne, V. M.; Hollins, P. *J. Electron Spectrosc. Relat. Phenom.* **1990**, *54*, 749.

(14) Lewis, G. J.; Roth, J. D.; Montag, R. A.; Safford, L. K.; Gao, X. P.; Chang, S.-C.; Dahl, L. F.; Weaver, M. J. *J. Am. Chem. Soc.* **1990**, *112*, 2831.

(15) Sheppard, N.; Nguyen, T. T. *Adv. Infrared Raman Spectrosc.* **1978**, *5*, 67.

(16) Shen, J.; Hill, J. M.; Watwe, R. M.; Spiewak, B. E.; Dumesic, J. A. *J. Phys. Chem. B* **1999**, *103*, 3923.

(17) Spiewak, B. E.; Dumesic, J. A. *Thermochim. Acta* **1997**, *290*, 43.

(18) Watwe, R. M.; Spiewak, B. E.; Cortright, R. D.; Dumesic, J. A. *Catal. Lett.* **1998**, *51*, 139.

(19) Shen, J. Y.; Hill, J. M.; Watwe, R. M.; Podkolzin, S. G.; Dumesic, J. A. *Catal. Lett.* **1999**, *60*, 1.

(20) Binder, K.; Landau, D. P. *Surf. Sci.* **1981**, *108*, 503.

(21) Masel, R. I. *Principles of Adsorption and Reaction on Solid Surfaces*; Wiley: New York, 1996; Chapter 4.

(22) Allen, M. P.; Tildesley, D. J. *Computer Simulation of Liquids*; Oxford University Press: New York, 1987.

(23) Hammer, B.; Nielsen, O. H.; Norskov, J. K. *Catal. Lett.* **1997**, *46*, 31.

(24) Flyvbjerg, H.; Petersen, H. G. *J. Chem. Phys.* **1989**, *91*, 461.

(25) Sharma, S. B.; Miller, M. T.; Dumesic, J. A. *J. Catal.* **1994**, *148*, 198.

(26) Guinn, K. V.; Rhoades, D. S.; Herz, R. K. *Surf. Sci.* **1997**, *393*, 47.

(27) de Menorval, L.-C.; Chaqroune, A.; Coq, B.; Figueras, F. *J. Chem. Soc., Faraday Trans.* **1997**, *93*, 3715.

(28) Bastein, A. G. T. M.; Toolenaar, F. J. C. M.; Ponec, V. *J. Catal.* **1984**, *90*, 88.

(29) Brandt, R. K.; Hughes, M. R.; Bourget, L. P.; Truszkowska, K.; Greenler, R. G. *Surf. Sci.* **1993**, *286*, 15.

(30) Augustine, R. L. *Heterogeneous Catalysis for the Synthetic Chemist*; M. Dekker, Inc.: New York, 1996; Chapter 2.

(31) Primet, M.; Elazhar, M.; Frety, R.; Guenin, M. *Appl. Catal.* **1990**, *59*, 153.

(32) White, J. M.; Akhter, S. *CRC Crit. Rev. In Solid State Mater. Sci.* **1988**, *14*, 131.

(33) Hahn, E.; Fricke, A.; Roder, H.; Kern, K. *Surf. Sci.* **1993**, *297*, 19.